RevMexAA (Serie de Conferencias), **15**, 62–67 (2003)

AN INSIDE-OUT VIEW OF BUBBLES

Y.-H. Chu, R. A. Gruendl, and M. A. Guerrero

Astronomy Department, University of Illinois, USA

RESUMEN

Los vientos estelares rápidos pueden barrer el medio interestelar y formar burbujas. La evolución de una burbuja es controlada principalmente por el contenido y condiciones físicas del viento estelar rápido chocado en su interior. Este gas caliente no había podido ser detectado de forma rotunda hasta el reciente lanzamiento de los observatorios espaciales de rayos X *Chandra* y *XMM-Newton*. Hasta la fecha, se ha detectado con certeza emisión difusa de rayos X en dos burbujas circunestelares creadas por vientos de estrellas Wolf-Rayet, en cuatro nebulosas planetarias y en dos superburbujas creadas por cúmulos estelares jóvenes. Los ajustes de modelos a los espectros de rayos X de estos objetos muestran que el gas caliente en burbujas circunestelares presenta temperaturas relativamente bajas ($\leq 3 \times 10^6$ K), mientras que las burbujas interestelares contienen fracciones significativas de gas más caliente ($\geq 5 \times 10^6$ K). En todos los casos se encuentran enormes discrepancias con las luminosidades en rayos X predichas por los modelos estándares de burbujas. En el futuro, los modelos teóricos de burbujas deberán examinar la validez de la conducción de calor e incluir de forma realista procesos microscópicos tales como la carga de masa de grumos densos de material y la mezcla turbulenta. La observación de NGC 6888 con ACIS-S a bordo de *Chandra* arrojará luz sobre estos procesos astrofísicos.

ABSTRACT

Fast stellar winds can sweep up ambient media and form bubbles. The evolution of a bubble is largely controlled by the content and physical conditions of the shocked fast wind in its interior. This hot gas was not clearly observed until the recent advent of *Chandra* and *XMM-Newton* X-ray observatories. To date, diffuse X-ray emission has been unambiguously detected from two circumstellar bubbles blown by WR stars, four planetary nebulae, and two superbubbles blown by young clusters. Model fits to the X-ray spectra show that the circumstellar bubbles are dominated by hot gas with low temperatures ($\leq 3 \times 10^6$ K), while the interstellar bubbles contain significant fractions of hotter gas ($\geq 5 \times 10^6$ K). In all cases, large discrepancies in the X-ray luminosity are found between observations and conventional models of bubbles. Future theoretical models of bubbles need to re-examine the validity of heat conduction and take into account realistic microscopic processes such as mass loading from dense clumps/knots and turbulent mixing. *Chandra* ACIS-S observation of NGC 6888 will shed light on these astrophysical processes.

Key Words: **H II REGIONS — ISM: BUBBLES — PLANETARY NEBULAE — STARS: MASS LOSS — STARS: WOLF-RAYET — X-RAYS: ISM**

1. INTRODUCTION: A BRIEF HISTORY OF BUBBLE STUDIES

In 1965, Johnson & Hogg reported three shell nebulae, NGC 2359, NGC 6888, and the nebula around HD 50896, and suggested that these nebulae were formed by interactions between the mass ejected by the central Wolf-Rayet (WR) stars and the ambient interstellar gas. In modern terminology, these shell nebulae are called "bubbles", the mass ejected by a WR star is "fast stellar wind", the shell nebula around HD 50896 has been cataloged as "S 308", and the ambient medium is designated "circumstellar medium", i.e., ejected stellar material.

The earliest theoretical treatments of interactions between fast stellar winds and the interstellar medium (ISM) were motivated by the central cavities and high-velocity motions observed in H II regions (Mathews 1966; Pikel'ner 1968; Pikel'ner & Schcheglov 1969; Dyson & de Vries 1972). Models of wind-ISM interaction were constructed specifically for shell nebulae around WR stars by Avedisova (1972), and a numerical calculation of wind-ISM interaction was provided by Falle (1975).

In 1974, Jenkins & Meloy reported *Copernicus* satellite observations of 32 early-type stars, which revealed ubiquitous shallow interstellar O VI absorption. To explain this O VI absorption, Castor, McCray, & Weaver (1975) modeled wind-ISM interaction and coined the term "interstellar bubble". Weaver et al. (1977) elaborated on this model and gained popularity because of their detailed description of the physical conditions and structure of a

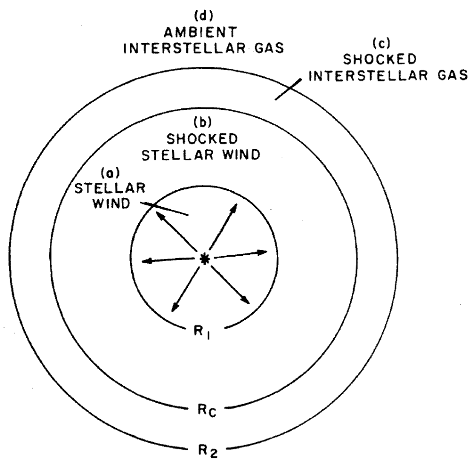

Fig. 1. Schematic structure of a pressure-driven interstellar bubble, from Weaver et al. (1977).

bubble and their specific characterization of X-ray emission and O VI column density expected from a bubble interior.

High-quality, high-resolution X-ray and far UV observations were not possible until the *Chandra X-ray Observatory*, *XMM-Newton X-ray Observatory*, and *Far Ultraviolet Spectroscopic Explorer* (*FUSE*) satellites were launched. It is finally possible to observe the hot gas in bubble interiors and critically examine the bubble models. The analysis of *FUSE* observations is complex, and it is premature to draw conclusions on the O VI absorption from bubbles. Therefore, in this paper we will concentrate only on X-ray observations of bubbles and compare them to model predictions.

2. BUBBLE MODELS

Most of the early models of bubbles assume that the stellar wind interacts with the ambient medium through momentum transfer and find that the shell expansion follows $r \propto t^{1/2}$, where r is the shell radius and t is the dynamic age (Mathews 1966; Pikel'ner 1968; Avedisova 1972; Steigman, Strittmatter, & Williams 1975). Their assumption of momentum conservation may be convenient for 1-D calculations in which the stellar wind does not get deflected. However, in 3-D space, momentum is a vector and the momentum flux of a stellar wind is null (otherwise the star itself would experience a rocket effect and gain momentum); it is unphysical to assume that the wind momentum in every specific direction is conserved.

Dyson & de Vries (1972) were the first to suggest that the expansion of a bubble is driven by the thermal pressure of the shocked wind in the bubble

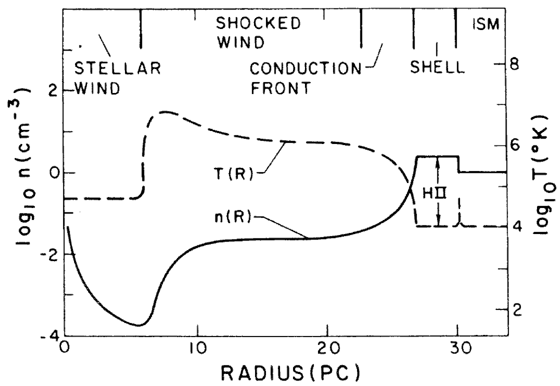

Fig. 2. Temperature and density profiles of a pressure-driven interstellar bubble, from Weaver et al. (1977).

interior, and follows the $r \propto t^{3/5}$ law. This formed the basis of the interstellar bubble model by Castor et al. (1975), who implemented heat conduction at the interface between the hot interior and the cool swept-up shell.

The basic structure of an interstellar bubble, illustrated in Figure 1, can be divided into four zones: (a) freely expanding stellar wind, (b) shocked stellar wind, (c) swept-up ISM, and (d) ambient ISM. The temperature and density structure of a bubble is illustrated in Figure 2. Two shocks are present in a bubble, an adiabatic shock at R_1, between zones (a) and (b), and an isothermal shock at R_2, between zones (c) and (d). The hot, shocked stellar wind and the swept-up ISM are separated by a contact discontinuity at R_c. In the shocked stellar wind layer, the temperature structure is modified by heat conduction, and the density at the outer edge is raised by mass evaporation across R_c from the dense swept-up interstellar shell. At the conduction front, the temperatures are high enough to produce collisionally ionized O^{+5}, which may be responsible for the interstellar O VI absorption detected in *Copernicus* observations of early-type stars.

For a pressure-driven bubble in a homogeneous ISM, the X-ray emissivity can be integrated over the volume with X-ray-emitting temperatures to determine the expected X-ray luminosity in soft energy band. As given by Chu et al. (1995), the expected X-ray luminosity in the 0.1 to 2.4 keV band can be expressed in wind parameters as $L_X \approx (2 \times 10^{35}\,\mathrm{erg\,s^{-1}})\xi\, L_{37}^{33/35} n_0^{17/35} t_6^{19/35}$, where ξ is the metallicity relative to the Solar value, L_{37} is the mechanical luminosity of the stellar wind in units of $10^{37}\,\mathrm{erg\,s^{-1}}$, n_0 is the ambient density in $\mathrm{cm^{-3}}$, and t_6 is the dynamic age in units of 10^6 yr. The X-ray luminosity can also be expressed in bubble parameters as $L_X \approx (1.6 \times 10^{28}\,\mathrm{erg\,s^{-1}})\xi\, n_0^{10/7} R_{\mathrm{pc}}^{17/7} V_5^{16/7}$,

TABLE 1

X-RAY OBSERVING FACILITIES

X-ray Observatory	Mission Duration	Imaging Spectrometer[a]	Angular Resolution	Energy Range (keV)
Einstein	1978–1981	IPC	120″	0.2–3.5
ROSAT	1990–1998	PSPC	30″	0.1–2.4
ASCA	1993–2001	SIS	150″	0.4–10
Chandra	1999–present	ACIS	1″	0.1–10
XMM-Newton	1999–present	EPIC	10″	0.1–15

[a]IPC: Imaging Proportional Counter; PSPC: Position Sensitive Proportional Counter; SIS: Solid-State Imaging Spectrometer; ACIS: Advanced Camera for Imaging and Spectroscopy; EPIC: European Photon Imaging Camera

where $R_{\rm pc}$ is the shell radius in units of pc, and $V_5 = 0.59 R_{\rm pc}/t_6$ is the shell expansion velocity in units of km s^{-1}.

Shell nebulae around WR stars are circumstellar bubbles consisting of stellar material ejected by the progenitors during a red supergiant (RSG) or luminous blue variable (LBV) phase; the circumstellar medium is far from homogeneous. The formation and evolution of WR bubbles have been hydrodynamically simulated by García-Segura, Langer, & Mac Low (1996a) and García-Segura, Mac Low, & Langer (1996b) for WR stars that have evolved through LBV and RSG phases, respectively. These models follow the same basic principles as Weaver et al. (1977) but have incorporated realistic stellar mass-loss history in their calculations. While these models are successful in reproducing the nebular morphologies, they find that the stellar wind luminosity expected from the observed bubble dynamics is often more than an order of magnitude lower than that derived from direct observations of the wind.

The clumpy morphology of WR bubbles implies that the stellar wind may be interacting with small fragments of nebular material, thus mass loading may be an important process that modifies the physical conditions of a bubble interior. Adiabatic bubbles with conductive evaporation and hydrodynamic ablation have been modeled by Pittard and collaborators (Pittard, Dyson, & Hartquist 2001a; Pittard, Hartquist, & Dyson 2001b). They find the X-ray emissivity and temperature profiles of a bubble interior can rise or fall toward the outer edge, depending on the ratio of wind mass to injected nebular mass.

Wind-blown bubbles are usually associated with massive stars; however, the formation of planetary nebulae (PNe) around low- and intermediate-mass stars is almost identical to that of a WR bubble (e.g., Kwok 1983; Chu 1993). Therefore, we will include PNe in our discussions in this paper.

3. X-RAY OBSERVATIONS OF BUBBLES

X-ray observations of wind-blown bubbles and PNe have been made with a number of satellites, of which the duration of the mission, instrument used, angular resolution, and photon energy range are summarized in Table 1. *Einstein* IPC observations detected diffuse X-ray emission from only one wind-blown bubble, NGC 6888 (Bochkarev 1988). Many detections of diffuse X-ray emission from interstellar bubbles in H II regions based on *Einstein* observations, e.g., the Orion Nebula (Ku & Chanan 1979), the Rosette Nebula (Leahy 1985), S 155 (Fabian & Stewart 1983), were later shown by *ROSAT* observations to be spurious, as the X-ray emission was resolved into stellar point sources (Chu 1994).

In Table 2, we summarize X-ray observations of bubbles and PNe made with "modern" X-ray satellites within the last decade. Objects with diffuse X-ray emission detected are listed without parentheses, and the non-detections are listed in parentheses.

3.1. *Diffuse X-ray Emission from WR Bubbles*

Diffuse X-ray emission has been detected from two WR bubbles, NGC 6888 and S 308. Figures 3 and 4 show optical [O III] and *ROSAT* PSPC images of these two bubbles (Wrigge, Wendker, & Wisotzki 1994; Wrigge 1999). Despite the limited angular resolution, the PSPC X-ray image of NGC 6888 shows clear limb-brightening. The X-ray morphology of S 308 cannot be easily visualized because the shell rim is occulted by the circular ring of the PSPC's window support structure. Analyses of the spectra extracted from these PSPC observations show that the hot gas in the interiors of these two WR bubbles is dominated by gas at $\sim 1.5 \times 10^6$ K. Wrigge (1999) also suggested a high-temperature, 2.8×10^7 K, component in S 308; however, this component may be contributed by the

TABLE 2

X-RAY OBSERVATIONS OF BUBBLES AND PLANETARY NEBULAE [a,b]

Observatory	Bubbles
ROSAT	NGC 6888, S 308, Omega Nebula, (NGC 2359), (NGC 3199), (NGC 6164-5), (NGC 7635)
Chandra	Rosette Nebula, Omega Nebula
XMM-Newton	S 308
	Planetary Nebulae
ROSAT	BD+30°3639, NGC 6543, Abell 30, (60+ PNe)
Chandra	BD+30°3639, NGC 6543, NGC 7027, (NGC 7293), (He 2-90), (M 1-16), (NGC 246)
XMM-Newton	NGC 7009

[a]Diffuse X-ray emission is detected only from objects listed without parentheses.

[b]References for objects with diffuse X-ray emission—Abell 30: Chu, Chang, & Conway (1997), Chu & Ho (1995); BD+30°3639: Kastner et al. (2000); NGC 6543: Chu et al. (2001); NGC 6888: Wrigge et al. (1994); NGC 7009: Guerrero, Gruendl, & Chu (2002); NGC 7027: Kastner, Vrtilek, & Soker (2001); Omega Nebula: Townsley et al. (2003), Dunne et al. (2003); Rosette Nebula: Townsley et al. (2001); S 308: Wrigge (1999), Chu et al. (2003).

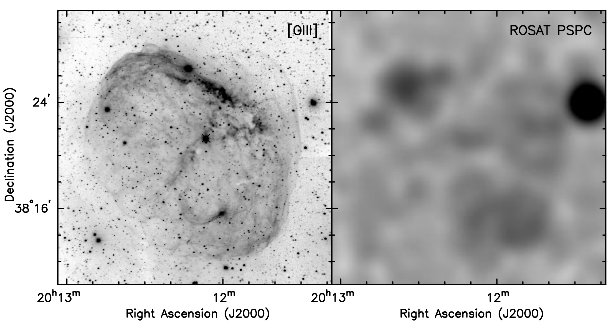

Fig. 3. Optical [O III] λ5007 image (left) and *ROSAT* PSPC image (right) of NGC 6888.

numerous unresolved point sources. *ASCA* observations of NGC 6888 detected an additional plasma component at $\sim 8 \times 10^6$ K (Wrigge et al. 1998).

These observations can be greatly improved by *Chandra* and *XMM-Newton*. We have been awarded a 100 ks *Chandra* observation of NGC 6888 in Cycle 4 that will be made in 2003. We have obtained 40 ks *XMM-Newton* observations of S 308, with the field of view covering the northwest quadrant of the bubble (see Figure 5). Although these *XMM* observations were affected by high background during 2/3 of the total exposure time, they show clearly a limb-brightened distribution of the X-ray emission from the interior of S 308. Most interestingly, a spatial gap is present between the outer edge of diffuse X-ray emission and the outer edge of [O III] emission, and this gap might be the conduction front that has been long sought after! The X-ray spectrum of S 308 (see Figure 6) is extremely soft, indicating a plasma temperature of only $\sim 1 \times 10^6$ K.

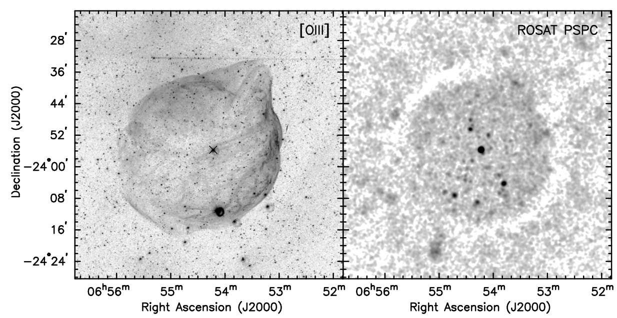

Fig. 4. Optical [O III] λ5007 image (left) and *ROSAT* PSPC image (right) of S 308.

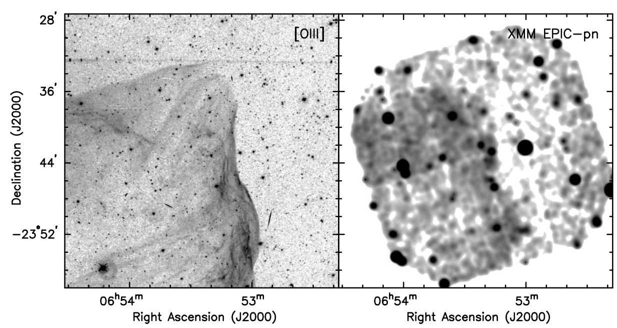

Fig. 5. Optical [O III] λ5007 image (left) and *XMM-Newton* EPIC image (right) of the northwest quadrant of S 308.

3.2. *Diffuse X-ray Emission from Planetary Nebulae*

More than 60 PNe have been observed by *ROSAT*, but only three nebulae show marginally extended X-ray emission (Guerrero, Chu, & Gruendl 2000). *Chandra* observations unambiguously resolved the diffuse X-ray emission from three PNe,

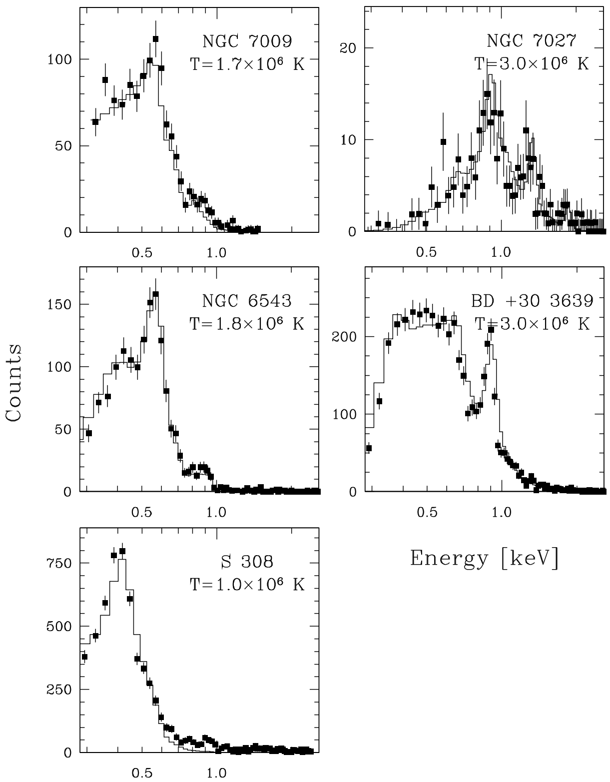

Fig. 6. *XMM-Newton* EPIC-pn and *Chandra* ACIS-S spectra of four PNe and one WR bubble.

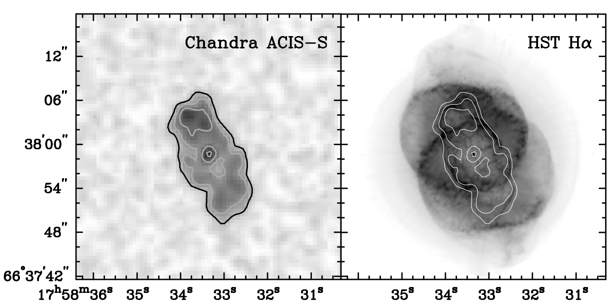

Fig. 7. *Chandra* ACIS image (left) and *HST* WFPC2 Hα image overlaid by X-ray contours (right) of the PN NGC 6543, the Cat's Eye Nebula.

and *XMM-Newton* observations resolved the diffuse X-rays from NGC 7009, see Table 2 for the names and references of these PNe. Figure 7 shows the most well-resolved PN, NGC 6543 (the Cat's Eye Nebula), where a limb-brightened morphology is clearly seen.

The X-ray spectra of the diffuse emission from four PNe are displayed in Fig. 6; all show thermal plasma emission. The best-fits to these spectra indicate plasma temperatures of 2 to 3×10^6 K and densities of $\sim 100\,\mathrm{cm}^{-3}$, from which we conclude that the hot gas in PN interiors is over-pressurized and drives the expansion of the optical nebular shell.

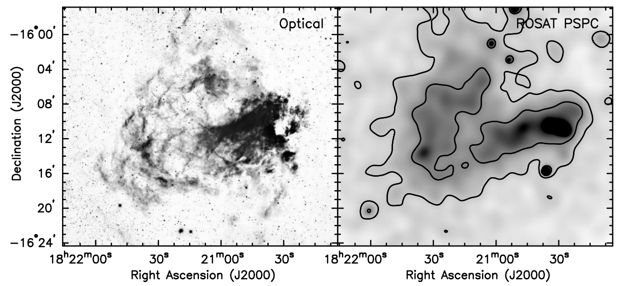

Fig. 8. Digitized Sky Survey red-band image (left) and *ROSAT* PSPC image (right) of the Omega Nebula.

3.3. *Diffuse X-ray Emission from Superbubbles*

Diffuse X-ray emission from quiescent superbubbles (without recent supernova blasts) is detected for the first time by *Chandra*—the Rosette Nebula and the Omega Nebula (Townsley et al. 2001, 2003). The diffuse X-ray emission from the Omega Nebula was in fact detected by *ROSAT*, but has never been reported. Figure 8 shows the *ROSAT* PSPC image and an optical image of the Omega Nebula; the diffuse X-ray emission fills the entire interior of this superbubble. As the ionizing cluster of the Omega Nebula is only $\sim 1 \times 10^6$ yr old, the hot gas must be produced solely by fast stellar winds.

The diffuse X-ray emission from the two interstellar superbubbles, the Rosette Nebula and the Omega Nebula, is qualitatively different from the diffuse emission from circumstellar bubbles, i.e., WR bubbles and PNe. First of all, the diffuse emission from the superbubbles does not show any limb-brightening. Second, X-ray spectra of the superbubbles show a high-temperature ($\sim 7 \times 10^6$ K) component in addition to the dominant component at $\sim 2 \times 10^6$ K. Finally, the densities of the hot gas in superbubbles are much lower than those in the interiors of WR bubbles or PNe.

4. OBSERVATIONS VERSUS THEORETICAL EXPECTATIONS

X-ray observations have detected diffuse emission from two WR bubbles, four PNe, and two young superbubbles. The typical physical properties of the X-ray-emitting gas derived from *Chandra* and *XMM-Newton* observations are listed in Table 3. The average X-ray spectrum of a bubble is weighted toward the densest X-ray-emitting region. As shown in Fig. 2, the density and temperature profiles in a bubble interior are anti-correlated, thus the brightest emission is expected to originate from regions with the lowest temperatures. The observed low plasma temperatures and limb-brightened morphology are fully consistent with this expectation. The observed

TABLE 3

PHYSICAL PROPERTIES OF HOT GAS IN BUBBLE INTERIORS

Bubble Type	T_e [10^6 K]	N_e [cm^{-3}]	L_X [erg s^{-1}]
Planetary Nebula	2–3	100	10^{31}–10^{32}
WR Bubble	1, 8?	10	10^{33}–10^{34}
Superbubble	2, 7	0.1	10^{33}–10^{34}

variations of plasma density among the three types of bubbles are also qualitatively consistent with the expectation from mass evaporation processes, as the plasma density should reflect the nebular density.

However, two outstanding discrepancies exist between the observations and theoretical predictions when they are compared *quantitatively*. First, the observed X-ray luminosities are 10 to 100 times lower than those predicted by pressure-driven bubble models using observed bubble dynamics, such as shell size, expansion velocity, nebular density, and stellar wind mechanical luminosity. Second, in a pressure-driven bubble model, the hot gas near the conduction front is dominated by nebular mass evaporated across the contact discontinuity, but the abundances of the X-ray-emitting gas in at least two PNe are consistent with those of the fast stellar winds instead of those of the nebular shells (Chu et al. 2001; Arnaud, Borkowski, & Harrington 1996). To resolve these problems, high-resolution observations of more bubbles are needed to study the detailed astrophysical processes, e.g., conduction evaporation, hydrodynamic ablation, and turbulent mixing. Our upcoming 100 ks *Chandra* observation of NGC 6888 may shed light on these processes.

REFERENCES

Arnaud, K., Borkowski, K. J., & Harrington, J. P. 1996, ApJ, 462, L75
Avedisova, V. S. 1972, Soviet Astronomy, 15, 708
Bochkarev, N. G. 1988, Nature, 332, 518
Castor, J., McCray, R., & Weaver, R. 1975, ApJ, 200, L107
Chu, Y.-H. 1993, in IAU Symp. 155, Planetary Nebulae, eds. R. Weinberger & A. Acker (Dordrecht: Kluwer), 139
_________. 1994, in AIP Conf. Proc. 313, The Soft X-ray Cosmos, eds. E. M. Schlegel & R. Petre (New York: AIP), 154
Chu, Y.-H., Chang, T. H., & Conway, G. M. 1997, ApJ, 482, 891
Chu, Y.-H., Chang, H., Su, Y., & Mac Low, M. 1995, ApJ, 450, 157
Chu, Y.-H., Guerrero, M. A., Gruendl, R. A., Williams, R. M., & Kaler, J. B. 2001, ApJ, 553, L69
Chu, Y.-H., & Ho, C. 1995, ApJ, 448, L127
Chu, Y.-H., et al. 2003, in preparation
Dunne, B. C., et al. 2003, in preparation
Dyson, J. E., & de Vries, J. 1972, A&A, 20, 223
Fabian, A. C., & Stewart, G. C. 1983, MNRAS, 202, 697
Falle, S. A. E. G. 1975, A&A, 43, 323
García-Segura, G., Langer, N., & Mac Low, M.-M. 1996a, A&A, 316, 133
García-Segura, G., Mac Low, M.-M., & Langer, N. 1996b, A&A, 305, 229
Guerrero, M. A., Chu, Y.-H., & Gruendl, R. A. 2000, ApJS, 129, 295
Guerrero, M. A., Gruendl, R. A., & Chu, Y.-H. 2002, A&A, 387, L1
Jenkins, E. B., & Meloy, D. A. 1974, ApJ, 193, L121
Johnson, H. M., & Hogg, D. 1965, ApJ, 142, 1033
Kastner, J. H., Soker, N., Vrtilek, S. D., & Dgani, R. 2000, ApJ, 545, L57
Kastner, J. H., Vrtilek, S. D., & Soker, N. 2001, ApJ, 550, L189
Ku, W. H.-M., & Chanan, G. A. 1979, ApJ, 234, L59
Kwok, S. 1983, in IAU Symp. 103, Planetary Nebulae, ed. D. R. Flower (Dordrecht: Reidel), 293
Leahy, D. A. 1985, MNRAS, 217, 69
Mathews, W. G. 1966, ApJ, 144, 206
Pikel'ner, S. B. 1968, Ap. Letters, 2, 97
Pikel'ner, S. B., & Shcheglov, P. V. 1969, Soviet Astronomy, 12, 757
Pittard, J. M., Dyson, J. E., & Hartquist, T. W. 2001a, A&A, 367, 1000
Pittard, J. M., Hartquist, T. W., & Dyson, J. E. 2001b, A&A, 373, 1043
Steigman, G., Strittmatter, P. A., & Williams, R. E. 1975, ApJ, 198, 575
Townsley, L. K., Feigelson, E. D., Broos, P. S., Chu, Y.-H., & Montmerle, T. 2001, BAAS, 199, 124.04
Townsley, L. K., et al. 2003, RevMexAA(SC), 15, 190 (this volume)
Weaver, R., McCray, R., Castor, J., Shapiro, P., & Moore, R. 1977, ApJ, 218, 377
Wrigge, M. 1999, A&A, 343, 599
Wrigge, M., Chu, Y.-H., Magnier, E. A., & Kamata, Y. 1998, Lecture Notes in Physics, 506, 425
Wrigge, M., Wendker, H. J., & Wisotzki, L. 1994, A&A, 286, 219

You-Hua Chu, Robert A. Gruendl, and Martín A. Guerrero: Astronomy Department, University of Illinois, 1002 W. Green Street, Urbana, IL 61801, USA (chu,Gruendl,mar@astro.uiuc.edu).